Probabilistic Characterization of Sweep and Ejection Events in Turbulent Flows: Insights from Direct Numerical Simulation Data

Kuan-Ting Wu[1], Christina W. Tsai*[2], and Meng-Jie Wu[1]

Key Points

- An integrated standard is applied to the available direct numerical simulation (DNS) turbulent flow data after UMZ edges were identified.
- Probabilistic characteristics of coherent structures such as the maximum height, wall-normal length and streamwise length can be determined.
- Durations of sweep and ejections events are demonstrated to follow a lognormal distribution.
- The occurrence ratio of sweep events in the large-scale motions (LSMs) is quantified from the DNS data.

[1] Graduate Research Assistant, Department of Civil Engineering, National Taiwan University, Taipei, Taiwan
[2] Professor, Department of Civil Engineering, National Taiwan University, Taipei, Taiwan, cwstsai@ntu.edu.tw (*Corresponding Author*)

Abstract

Turbulent boundary layers are populated by a hierarchy of recurrent structures normally referred to as "coherent structures." Among others, ejection and sweep events are critical coherent structures of large-scale motions in turbulent flows. This study focused on gaining a better understanding of the spatial-temporal probabilistic characteristics of sweep and ejection events. The existence of uniform momentum zones (UMZs) is demonstrated to affect the spatial distribution of large-scale motions, and the ejection and sweep events tend to present near UMZ edges. On the basis of such observations, we considered the effect of UMZ edges on the presence of ejection and sweep events. In the current study, UMZ detection was employed to identify coherent structures. Several criteria for identifying coherent structures are revisited, and an integrated standard is applied to the available direct numerical simulation (DNS) turbulent channel flow data after UMZ edges were determined. Based on the integrated criterion for distinguishing ejection and sweep events, one can determine the probabilistic characteristics of coherent structures such as the maximum height, wall-normal length and streamwise length. Physical insights from DNS data such as joint probability density functions of wall-normal length and streamwise length can be established. The attached and detached features of the sweep and ejection coherent structures can then be classified and characterized, respectively. Durations of sweep and ejections events were demonstrated to follow a lognormal distribution in this study. The occurrence ratio of sweep events in the large-scale motions (LSMs) was quantified from the DNS data.

***Keywords*:** turbulent flows; coherent structures; conditional velocity decomposition; probability distributions; large scale motions; DNS data

1. Introduction

Sediment transport in open channel flow has a significant impact on the siltation of rivers, reservoirs, and artificial channels, and it is one of the major topics studied in the water resources realm. Despite the intensive investigation done in the past, the transport mechanism of sediment particles seems to have reached a stage where further progress may depend on a more comprehensive understanding of the chaotic and intermittent behavior of turbulence. Among others, the existence of coherent structures in wall-bounded turbulent flows has been confirmed. Such turbulent structures play a dominating role not only in the movement of sediment particles but also in determining mean flow, stress and other statistical properties. For example, the coherent structures near the bed tend to have a large momentum exchange, leading to increased Reynold shear stress near the bed (MacVicar & Roy, 2007; Truong & Uijttewaal 2019; and Wang et al. 2021). Zhong et al. (2016) discovered that strong super-streamwise vortices might cause erosion and sedimentation in the downwelling and upwelling sides, respectively.

It has been shown that transport of sediment particles is closely related to some coherent structures defined as the ejection (Q2) and sweep (Q4) events (Chang et al., 2011; Dwivedi et al., 2011; Muste and Yu, 2005). Hurther and Lemmin (2003) indicated that ejection (Q2) and sweep (Q4) events tend to entrain the particles into suspension and to move particles near the bed, respectively. Lelouvetel et al. (2009) proposed that over 70% of coherent structures observed at particle incipient motion in turbulent flows can be classified as ejections (Q2) and sweeps (Q4). The influence of ejection and sweep events on sediment entrainment is reported (Nino and Garcia, 1996; Dwivedi et al., 2011). These two coherent structures also influence the instantaneous local

sediment concentration in the near-wall region (Cellino and Lemmin, 2004; Noguchi and Nezu, 2009; Salim et al., 2017).

Moreover, these coherent structures disturb sediment particles for a particular period and carry particles over long distances, resulting in the temporal and spatial correlations of flow velocities in the flow field (Cellino & Lemmin 2004; Okamoto, Nezu & Katayama 2010). Chen, Sun & Zhang (2013) presented a model that is based on the fractional advection-diffusion equation to account for the long distances over which sediment particles are carried by large turbulent structures. More recently, Tsai and Huang (2019) and Tsai et al. (2021) have shown that when particles transport within time-persistent turbulent flow structures, the movements of the sediment particles may exhibit persistency that depends on the various temporal durations of turbulent flow structures.

Based on the observations mentioned above, the coherent structures are found to be critical in affecting the probabilistic behavior of sediment particles. It is desirable to better understand and quantify the spatial and temporal characteristics of turbulent flows, particularly the sweep and ejection events so that the influence of turbulent coherent structures on sediment particle movement can be more precisely evaluated. This study aims at answering the following fundamental questions. (1) What is the probability distribution of the maximum height of the event occurrences? (2) How to describe the geometrical structure (spatial scales) of the sweep and ejection events in a probabilistic manner? And (3) How to statistically characterize the duration (temporal scales) of the sweep and ejection events?

2. Turbulent Coherent Structure and Uniform Momentum Zones (UMZs)

In turbulence research, it is acknowledged that deconstructing complex turbulence into more characteristic elementary components would provide additional information about its nature. On the basis of their laboratory experiments, Grass (1971) and Wallace et al. (1972) indicated that turbulence is generated by intermittent coherent structures (burst cycles) near the boundary. Since then, many studies have presented evidence that the turbulent boundary layer (TBL) is populated by a hierarchy of coherent structures such as low- and high-speed streaks (Offen & Kline, 1975), ejections and sweeps (Wallace et al., 1972), streamwise vortices (Blackwelder & Eckelmann, 1979), hairpin vortices (Offen & Kline, 1975) large-scale bulges (Falco, 1977), hairpin vortex packets (Adrian et al., 2000), very large-scale motions (VLSMs) (Kim & Adrian, 1999), and superstructures (Hutchins & Marusic, 2007). In their extensive study on the TBL structure, Smits et al. (2011) summarized the scaling laws, generation and interaction mechanisms, and their roles in the production and dissipation of these coherent structures. Moreover, Adrian and Marusic (2012) analyzed hairpin and packet-like structures to determine these structural properties.

Regarding the characteristic spatial scales (e.g., geometry) of turbulent structures, Meinhart and Adrian (1995) first highlighted the existence of large and irregularly shaped regions of uniform streamwise momentum zones (hereafter, UMZs), regions of relatively similar streamwise velocity with coherence in the streamwise and wall-normal directions. It is observed that these UMZs generally encapsulated the near-wall region. Accordingly, the boundary layer is divided into several zonal structural arrangements and demarcated by thin interfacial layers of strong shear, where most of the vorticity is clustered in the TBL (Adrian et al., 2000; Eisma et al., 2015). The relationship of large-scale motions (LSMs) such as ejection and sweep events with the existence of UMZs is debated. Based on these works, de Silva et al. (2016) provided insight into how

instantaneous phenomena such as a zonal-like structural arrangement can be separated by UMZ edges.

de Silva et al. (2017) also provided a detection criterion that had previously been used to locate UMZs and demonstrated the application of this criterion to estimate the spatial locations of the edges that demarcate UMZs. They also demonstrated the regulation of the presence of ejection (Q2) and sweep (Q4) events, which occur below and above the interface, respectively. Hence, the LSMs' spatial distribution is confirmed to be affected by the existence of UMZs.

Owing to advances in particle image velocimetry (PIV) and direct numerical simulation (DNS), which researchers of turbulence structures in TBLs can draw from, the presence of a pronounced zonal-like structure in instantaneous fields of streamwise velocity fluctuations has been revealed. That is, the TBL includes several regions of roughly uniform streamwise velocity magnitudes, called the UMZ. Meinhart and Adrian (1995) observed that a UMZ edge separates the neighboring UMZs with a strong shear originating from concentrated patches of vortices. de Silva et al. (2016) also demonstrated that sudden step-like jumps exist in the streamwise flow velocity profile. Therefore, streamwise velocities within UMZs are bounded by distinct step changes in streamwise momentum, which indicate that shear layers of intense vorticity separate each zone. Specifically, these UMZs are demarcated by thin interfaces of strong shear that indicate a large proportion of the vorticity is clustered in the turbulent boundary layer (TBL).

The organized vortical structures that contort UMZ interfaces are a manifestation of ejection events and sweep events around the interface (Ganapathisubramani et al., 2003; Saxton-Fox & McKeon, 2017; Tomkins & Adrian, 2002), demonstrating that UMZ edges and the spatial distribution of LSMs affect each other. In this study, discrimination of the interfaces of UMZs is an essential step in estimating the spatial-temporal characteristics of LSMs. **Figure 1** illustrates the potentially impacted region in TBL on sediment particles due to turbulent coherent structures.

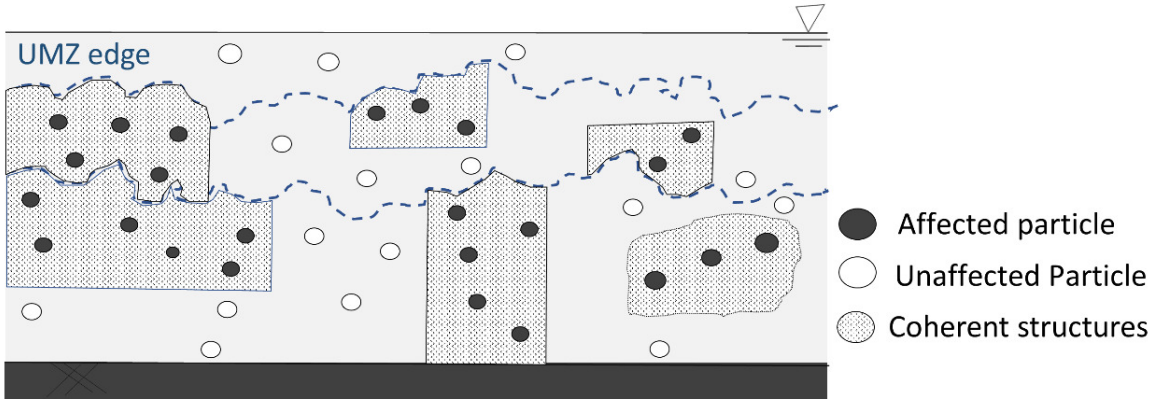

Figure 1. Conceptual vertical section with an ejection event

3. Description of DNS data

Lee and Moser (2014) used DNS to obtain channel flow data, which are available online in the Johns Hopkins Turbulence Databases (JHTDB; http://turbulence.pha.jhu.edu). The simulation we analyze here is DNS of incompressible turbulent flow between two parallel planes, and no-slip condition/no-penetration boundary condition is applied on the wall. Details of the experimental parameters of JHTDB are summarized in **Table 1**. It should be mentioned that the time step we utilized is 0.05 sec, which is smaller than the time scale of experimental physical

phenomena, i.e., the duration of coherent structures. Based on LeHew et al. (2013) regarding the lifespan of coherent structures, the shortest duration they observed is about 0.1 sec. The time step (0.05 sec) in this study is suitable for capturing the temporal distribution of coherent structures.

Table 1. Experimental parameters of JHTDB employed. L_x and L_y correspond to the field of view of the streamwise wall-normal plane, and h is the half channel height. It should be noted that because $U_c \neq U_\infty$ in JHTDB, we assume the maximum of measured velocity equal to U_∞.

Friction velocity Reynolds number Re_τ	Viscosity ν	Domain Length $L_x \times L_y$	Centerline velocity $U_c(ms^{-1})$	Friction velocity $u^*(ms^{-1})$	half channel height $\delta\ (m)$
5186	8×10^{-6}	$8\pi \times 2$	1.1	0.041	1.0

This database was selected because it includes data on wall-bounded turbulent flows with high Reynolds numbers. Moreover, the DNS feature of this database can provide detailed information about the generating role of LSMs that would not otherwise be available. Therefore, the current study aimed at gaining further physical insight into the probabilistic spatial and temporal scales and other characteristics of sweep and ejection coherent structures in turbulent flows.

4. Detection of UMZs

Instantaneous UMZs were detected using the methodology of Adrian et al. (2000) and de Silva et al. (2016, 2017). According to these studies, UMZs were detected from the local maxima in the probability density functions (PDFs) of the streamwise velocity components. These distinct local maxima, which are related to the streamwise momentum of each UMZ in the PDFs, represent large regions of the flow that develop downstream at relatively constant velocity magnitudes or modal velocities. The magnitude of the streamwise velocity that demarcates each detected UMZ is approximated by the midpoint between modal velocities of neighboring UMZs. **Figure 2** displays the detection criterion employed in this study. **Figure 2**(b)presents an instantaneous velocity field obtained from JHTDB whose $Re_\tau \approx 5{,}200$. The corresponding PDF of the streamwise velocity is presented in **Figure 2**(a), where the peaks of this PDF are referred to as modal velocities (indicated by ○ symbols). Notably, $y^+ = 0$ represents the location in the upmost boundary layer, whereas $y^+ = 5{,}500$ indicates the location on the boundary.

In this study, the spatial location of the UMZ was determined using a streamwise velocity magnitude (**Figure 2**). Notably, de Silva et al. (2016) estimated the location of the turbulent–non-turbulent interface (TNTI) by using a constant streamwise velocity magnitude of $97\%U_\infty$ to minimize the influence of applying the various detection criteria used for the TNTI and the UMZ edges. However, because the streamwise velocity magnitude of $97\%U_\infty$ is insufficient for clearly drawing the TNTI, the TNTI is not included in our discussion. **Figure 2**(a) displays three clear peaks in the PDFs (modal velocities), whose corresponding UMZs are also detectable (**Figure 2**(b)). The detected UMZ edges are represented by the solid lines, which are overlaid on iso-contours of streamwise velocity. Therefore, after the detection of UMZ edges, two UMZ edges appear in this flow field. As indicated, the location of the upper UMZ edge appears at $y^+ \approx 3{,}900$,

and the location of the lower UMZ edge appears at $y^+ \approx 1{,}600$. Srinath (2017) proposed a threshold which is y^+ is larger than $0.1\delta^+ \approx 500$; then the region called the outer region. Thus, compared with the general stratification of TBL, the UMZ edges exist in the outer region of TBL.

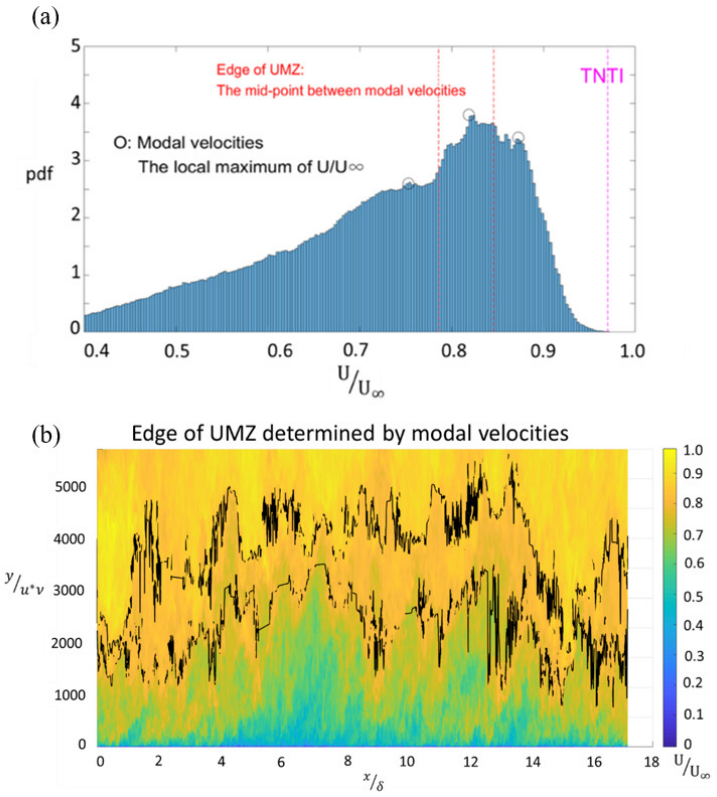

Figure 2. Illustration of the detection of instantaneous UMZs. (a) The corresponding histogram of U/U_∞; vertical dashed lines represent the streamwise velocity of the detected UMZ edges. (b) UMZ edges determined using modal velocities overlaid on iso-contours of streamwise velocity (U). the color bar for the study area ($0 \leq x/\delta \leq 17, 0 \leq y^+ \leq 5{,}500$) is on the right.

5. Instantaneous Flow Velocity Decomposition

Before directly extracting the characteristics of coherent structures from the database, we conducted velocity decomposition to quantify the mean velocity and corresponding velocity fluctuation. Based on the magnitude of the mean fluid velocity and its fluctuations, coherent structures can be extracted from the DNS data. Reynolds decomposition is widely used for analyzing velocity fields. Accordingly, Reynolds decomposition, whose general form is presented in Equation 1, is typically employed to evaluate the fluctuating component of velocity in the analysis of velocity fields in a certain region of the TBL.

$$u = \bar{u} + u' \quad (1)$$

where u is total flow velocity, $\bar{u}$ is mean flow velocity, and u' is the velocity fluctuation. The distribution of u' is dependent on the properties of the flow field.

The statistical properties of flow velocities involve fluid particle movement information. In the current study, such information was used to represent the flow structures in the wall-bounded

flow. However, the analyses were extended into the whole TBL region, where streamwise velocity becomes lower nearer to the wall; therefore, the near-wall sweep event might be eliminated because of the use of a conventional mean. That is, under the Reynolds decomposition, both ejection and sweep events might be reduced to background fluctuation under the threshold of the traditional mean.

The characterization of each flow region is independent of all other regions, which cannot be isolated under the Reynolds decomposition. Thus, in the current study, the conditional mean might be an appropriate method for decomposing the total velocity. The separation of turbulent and non-turbulent regions using different mean velocities was first attempted by Antonia (1972) and Hedleyt and Keffer (1974). Subsequently, Antonia et al. (1975), Fabris (1979), and Gutmark and Wygnanski (1976) observed various zonal mean velocities in different respective regions and defined the fluctuation of velocity regarding the zonal mean velocities for each respective region instead of using Reynolds-averaged mean velocities.

Recently, Kwon et al. (2016) and Lee et al. (2017) proposed a new decomposition approach in which the mean velocity is a function of not only the wall-normal distance but also the height of the TNTI interface (i.e., it is the outermost UMZ edge in the TBL). In our application, we followed their procedure and treated the mean velocity as a function of both the wall-normal distance and the height of UMZ edges. Our results are presented in **Figure 3**(a), where the red line represents the ensemble mean of the conditional mean velocity profiles, which satisfy the values of the UMZ edges represented by the blue dotted lines.

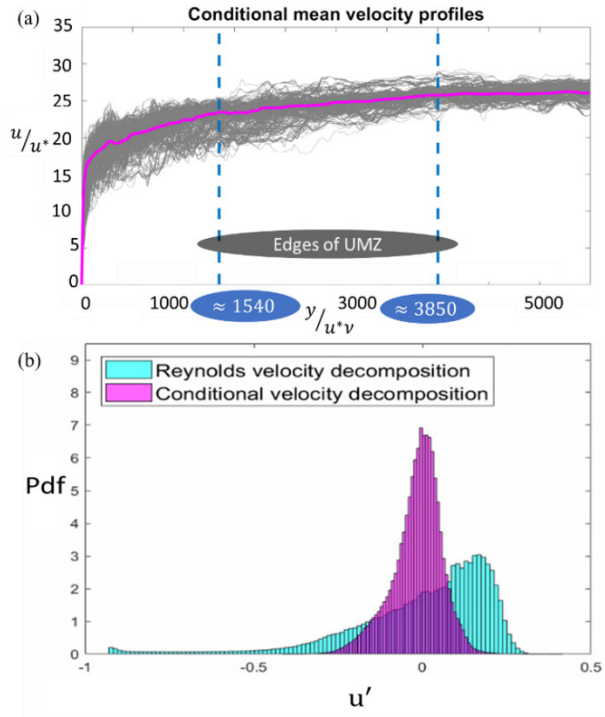

Figure 3. (a) Conditional mean velocity profiles. (b) Histograms of streamwise velocity fluctuation.

Figure 3(b) displays the comparison of the PDF of streamwise velocity fluctuations based on the Reynolds and conditional decomposition. Here, the blue PDF represents the distribution obtained from Reynolds velocity decomposition, whose range of fluctuations is wider than that of

conditional velocity fluctuations (the red PDF), which were obtained by considering the spatial variation of the mean velocity. Therefore, considering the spatial distribution of structures yields a conditional velocity decomposition that is more suitable for capturing the coherent structures than is Reynolds decomposition, in which the mean velocity is a single value. After obtaining the conditional mean velocity profile, we further applied the identified criterion, which was used to capture the physical properties of the coherent structures.

6. Identification of Coherent Structures

Identifying the coherent structures in a TBL depends on knowing the mechanics of turbulence, which is provided by understanding the characteristics of a group of eddies that sufficiently manifest the flow dynamics. Accordingly, this section examines the dynamics of the TBL in terms of the temporal evolution of coherent structures. Coherent structures are organized in space and persistent in time. However, the literature provides various criteria for identifying coherent structures. Several well-known methods are revisited, and an integrated standard is applied.

6.1 Criteria for Identifying Coherent Structures: Q Criterion

Although no consensus has been reached on the mathematical definition, coherent structures are intuitively accepted by the fluid dynamics community as three-dimensional (3D) tube-shaped structures with spatially limited distributions of concentrated vorticity (Jeong et al., 1997; Kaftori et al., 1994; Robinson, 1991). The vorticity magnitude was first used to identify the vortex tube (She et al., 1990). However, because the vorticity method was insufficient for distinguishing between vortex cores and shear motions, the method was later replaced by more robust criteria based on the local velocity gradient tensor, which was used to identify the vortex tube in 3D velocity fields (Hunt et al., 1988; Jeong & Hussain, 1995; Nagaosa, 1999).

Hunt et al. (1988) developed the Q criterion for a full velocity gradient tensor in incompressible flows; the second invariant Q can be written as

$$\mathrm{Q} = \frac{1}{2}(\|\Omega\|^2 - \|S\|^2) \tag{2}$$

where Ω is the rate-of-rotation tensor corresponding to pure rotational motion and S is the rate-of-strain tensor corresponding to pure irrotational motion.

$$\Omega = \frac{1}{2}[\nabla U - (\nabla U)^T] \tag{3}$$

$$\mathrm{S} = \frac{1}{2}[\nabla U + (\nabla U)^T] \tag{4}$$

Hence, the second invariant is a local measure of the excess rotation rate relative to the strain rate. For a two-dimensional (2D) velocity gradient tensor, Equation 1 can be simplified to

$$Q = -\frac{\partial u}{\partial y}\frac{\partial v}{\partial x} - \frac{1}{2}\left(\frac{\partial u}{\partial x}\right)^2 - \frac{1}{2}\left(\frac{\partial v}{\partial y}\right)^2 \tag{5}$$

where connected regions of positive Q are defined as vortices, and $Q > 0$.

6.2 Criteria for Identifying Coherent Structures: λ_{ci} criterion

The use of vorticity and kinematics implied by the velocity gradient tensor has been reported. Zhou et al. (1999) proposed the use of the imaginary part of the complex eigenvalue of

the local velocity gradient tensor as an unambiguous measure of rotation and the commonly named swirling strength. Unlike vorticity, swirling strength, λ_{ci}, (i is not an index in this definition but an abbreviation for the word "imaginary") does not highlight regions of intense shear. The swirling strength criterion has been demonstrated to be an adequate identifier of vortex cores (Adrian et al., 2000).

Similar to the 3D form, the 2D form of the λ_{ci} criterion is based directly on the Δ criterion. On the basis of the 2D velocity gradient tensor, the λ_{ci} indicator can be computed as

$$\lambda_{ci} = \frac{1}{2}\sqrt{-4\frac{\partial u}{\partial y}\frac{\partial v}{\partial x} - \left(\frac{\partial u}{\partial x} - \frac{\partial v}{\partial y}\right)^2} \quad (6)$$

6.3 Criteria for Identifying Coherent Structures: λ_2 criterion

Nagaosa (1999) revealed that a layer-like coherent structure is frequently misidentified as a vortex tube, particularly in the near-wall region, when vorticity is used as an indicator. To avoid such mistakes, the researchers applied the indicator developed by Jeong and Hussain (1995). The aforementioned indicator is based on the observation that a local pressure minimum corresponds well with the vortex center, except in the presence of strong, unsteady, and viscous effects. Moreover, on the basis of the 2D velocity gradient tensor, λ_2 can be computed as

$$\lambda_2 = \frac{\partial u}{\partial y}\frac{\partial v}{\partial x} + \frac{1}{2}\left[\left(\frac{\partial u}{\partial x}\right)^2 + \left(\frac{\partial v}{\partial y}\right)^2 + \left|\frac{\partial u}{\partial x} + \frac{\partial v}{\partial y}\right|\sqrt{\left(\frac{\partial u}{\partial x} - \frac{\partial v}{\partial y}\right)^2 + \left(\frac{\partial u}{\partial x} + \frac{\partial v}{\partial y}\right)^2}\right] \quad (7)$$

where the region satisfying $\lambda_2 < 0$ can be identified as vortices.

Coherent structures such as well-organized quasi-streamwise vortex tubes or bursting events are intermittently generated by near-wall turbulence. Therefore, a spatial illustration after the Q criterion, λ_{ci} criterion, or λ_2 criterion is applied as an overview of vortices. If structures such as sweep and ejection events must be distinguished, then relevant criteria should be integrated to provide a more rigorous definition of coherent structures.

6.4 Criteria for Identifying Coherent Structures: H Criterion

Ferreira et al. (2002) and Lu and Willmarth (1973) defined a threshold that allows the commonly named hole-size H to be used for detecting ejection and sweep events. Yoon et al. (2020) then defined the coherent structures of u as groups of connected points where $u > \mathrm{H} \times u_{rms}$ and $u < -\mathrm{H} \times u_{rms}$ in instantaneous flow fields, where H is identified. However, different recommendations for the value of H have been proposed, affecting the result of structure detection. For example, H = 1.2, 1.5,1.7, 1.75, 2.5, and 3 have all been proposed (Franca et al., 2014; Liu et al., 2016; Lozano-Durán et al., 2012; Nezu et al., 1994; Séchet & le Guennec, 1999; Yoon et al., 2020). In particular, Lozano-Durán et al. (2012) noted that the threshold depends on the wall distance. Therefore, the authors introduced the percolation theory to generate the statistics of connected components on a random graph. This theory can also be applied to extract the volume of connected eddies. del ÁLamo et al. (2006), Moisy and Jiménez (2004), and Yoon et al. (2020) first attempted to identify the vorticity and dissipation structures in isotropic turbulence, channels, and zero pressure gradient TBLs, respectively.

The percolation diagram of the identified coherent structures (**Figure 4**) was used to select H. The blue line is the ratio of the volume of the largest identified eddies, V_{max}, to the total volume V, satisfying the value of H from 0.1 to 3, whereas the red line indicates the total number of identified objects (N) normalized by its maximum (N_{max}), whose peak appears at H ≈ 1.5. This behavior is consistent with the result of Yoon et al. (2020). The normalized volume ($^{V}/_{V_{max}}$) increases as H decreases. As H decreases, new structures arise, or some of the previously detected objects gather. The balance between the two effects yields the peak in the variation of $^{N}/_{N_{max}}$. However, the value of H is a function of wall distance, as previously mentioned. Although the whole TBL is considered here, other studies have considered only a particular region in the TBL; therefore, our results do not reveal the peak clearly. In the present study, despite the unclear peak, H ≈ 1.5 was selected on the basis of the percolation transition.

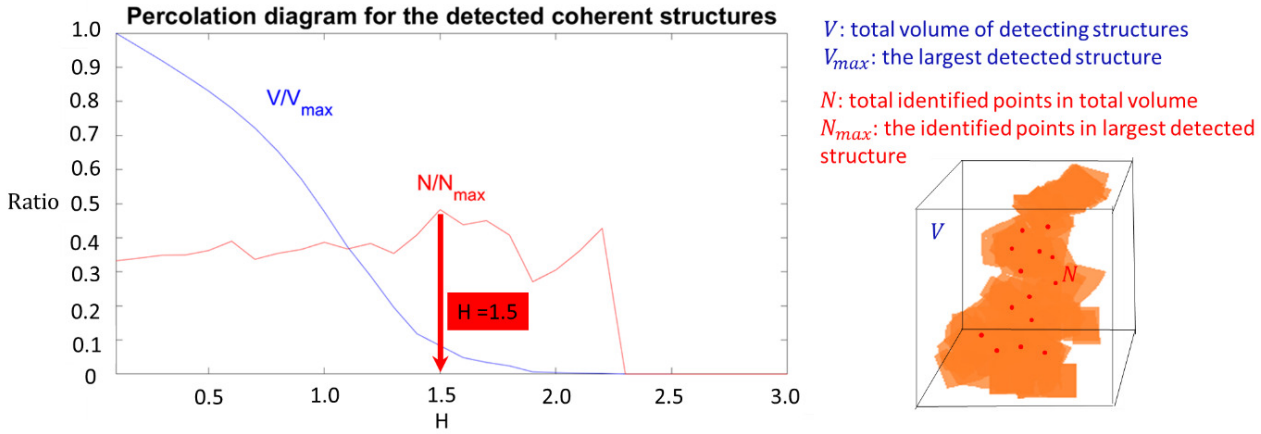

Figure 4. Percolation diagram for the detected coherent structures. The variations within the total volume (V) and the total number (N) of objects are displayed.

6.5 Criterion Comparison and Selection

Comparing Equations 5–7, Q, λ_{ci}, and λ_2 satisfy the following condition:

$$\frac{\partial u}{\partial y}\frac{\partial v}{\partial x} < 0 \qquad (8)$$

To explore the similarities and differences among these equations, Chen et al. (2015) compared the aforementioned criteria using planar velocity fields extracted from both DNS and PIV datasets. Moreover, the researchers revealed that a mathematical relationship between these criteria could interpret the disparity among the identification of coherent structures. According to Equation 5–7, Q > 0 is a subgroup of $\lambda_{ci} > 0$, and $\lambda_2 < 0$ is a subgroup of Q > 0. Therefore, λ_2 tends to eliminate the relatively weak vortices and make visible a snapshot of the structure identification, so we have used it herein. As mentioned, the structures discussed here are the commonly named Qs events, which are detected using quadrant analysis. However, Ferreira et al. (2002) first revealed that quadrant analysis might lead to inadequate features. An individual turbulent event may be detected as a series of separate smaller events. Section 5.4 presented the modification of the quadrant threshold method. Comprehensively, the applied threshold criteria are as follows:

Ejection:

$$Q_2 = \{(u < -1.5 \times u_{rms}) \wedge (u' < 0) \wedge (\lambda_2 < 0) \wedge (v' > 0)\}$$

Sweep:

$$Q_4 = \{(u > 1.5 \times u_{rms}) \wedge (u' > 0) \wedge (\lambda_2 < 0) \wedge (v' < 0)\}$$

Figure 5 illustrates the extracted coherent structures in the flow field based on the integrated criterion.

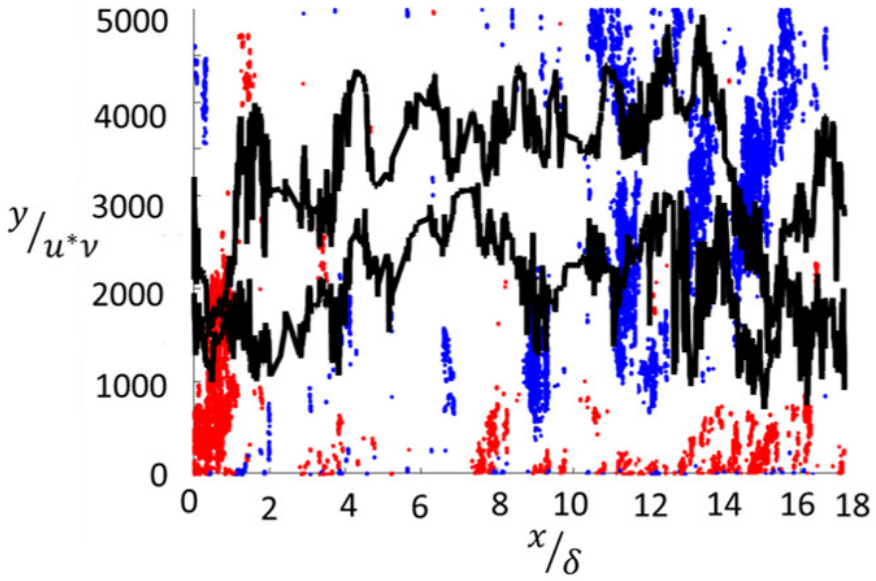

Figure 5. Coherent structures are identified in a snapshot from the JHTDB. The blue points represent the structures classified as sweep events, and the red points represent the structures classified as ejection events. The black lines represent the UMZ edges.

6.6 Tracking the Duration of Sweep and Ejection Events

Time-resolved data were used to track the events over time, enabling the production and dissipation of each event to be identified and the duration of each event to be determined. This section describes the method used for tracking the sweep and ejection events over time. On the basis of the assumption used by Fiscaletti and Ganapathisubramani (2018), if two events ev_1 and ev_2 are detected consecutively, and the following condition holds, we treat them as the same event:

$$d_{cent} < D_{box} \quad (9)$$

where d_{cent} is the distance between the centroids of ev_1 and ev_2, and D_{box} is the diagonal of the smallest rectangle, including all points of ev_1, as depicted in **Figure 3**(a) (Yoon et al., 2020).

7. Characterization of LSMs in the TBL

Here, ejection and sweep events are referred to as LSMs. This section analyzes the results of the JHTDB application of the detection criterion described in section 6.1 to determine the spatial-temporal distribution of LSMs.

7.1 Spatial Distribution of Events

Regarding the spatial distribution of ejection and sweep events, Dennis and Nickels (2011) conducted their analysis on the quasi-instantaneous 3D velocity fields of a TBL and observed that strong vertical velocity fluctuations are adjacent to the large flow structures. Their results imply that ejection and sweep events occur around structures with low and high streamwise velocities, respectively. Tsai and Huang (2019) treated the histogram of the maximum heights reached by structures with low and high streamwise velocities as representing the probabilities of ejection and sweep events at various flow elevations. Dennis and Nickels (2011) suggested that the gamma distribution can provide the best fit to the histogram of the maximum height.

In the current study, the structural properties, such as maximum height, streamwise and wall-normal length, and duration, were extracted from the JHTDB. The flow condition under which the JHTDB data were obtained differs from that of Dennis and Nickels (2011), causing the structures to characterize somewhat differently.

Figure 6 presents the probability density function of the maximum height of (**a**) ejection and (**b**) sweep events. As presented in the figure, a low point at y^+ exists between 1,100 and 2,200, where the upper UMZ edge is located. Moreover, the maximum height in the region between 1100 and 2200 in (a) and above 4,400 in (b) is similar to that described by de Silva et al. (2017), who observed that sweep events are generally located above the UMZ edges, and ejection events are generally located under the UMZ edges. In the current study, the two UMZ edges are located at $y^+ \approx 1{,}540$ and $y^+ \approx 3{,}850$. After the sweep and ejection events occurred above the upper UMZ edge and below the lower UMZ edge, respectively, they populated the entire UMZ region. This phenomenon is consistent with Lozano-Durán and Jiménez (2014), who claimed that ejection events appear in the near-wall region and rise, whereas sweep events appear away from the wall and drop.

If an event occurs, its maximum height must be determined to be its upper boundary, depending on the distribution presented in **Figure 6**(a & b). However, its lower limit is determined in one of two manners, one of which was made evident by de Silva et al. (2017), who presented a scenario in which the ejection and sweep events are likely to appear below and above the interface, respectively. **Figure 6**(c & d) displays the distribution of the vertical lengths of LSMs. Because the whole flow field is divided into three parts in the wall-normal direction after consideration of the UMZ edges, the scale of wall-normal length (L_y) in this analysis is consistent with the results of Yoon et al. (2020), who found that most L_y values range from 0.4δ to 0.6δ.

Tsai and Huang (2019) postulated that the flow region below the sampled maximum height is affected by LSMs. This work established that the LSM length scales in the vertical direction are also affected by the UMZ edges.

Regarding the streamwise LSM length, the properties of each event were extracted directly from the dataset. The histogram of streamwise length represents the probability that the range in the streamwise direction is influenced by ejection and sweep events (**Figure 6**(e & f)). Because of

the application of the criterion proposed by Fiscaletti and Ganapathisubramani (2018) into the spatial resolution of the identification of coherent structures, two consecutive events could be merging into a larger event. Although Dennis and Nickels (2011) used an exponential distribution to represent the streamwise LSM lengths, the distribution of both ejection and sweep events favored the more extended event.

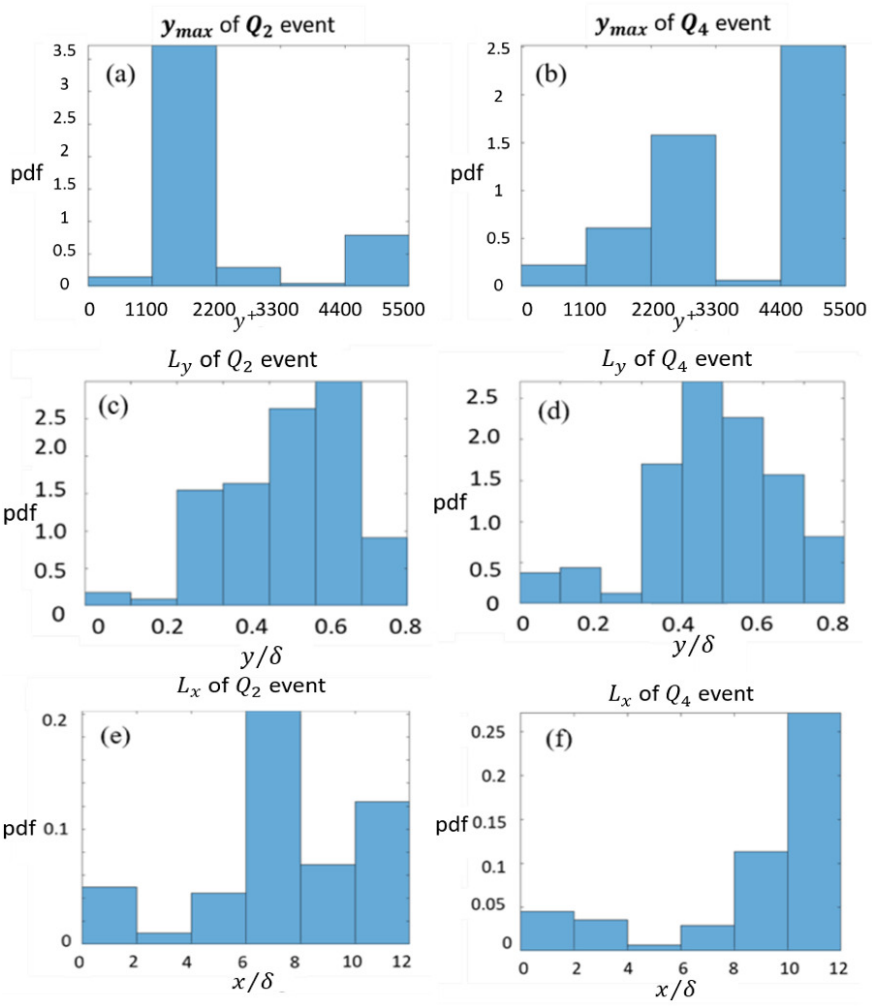

Figure 6. Probability density functions of the maximum height of (**a**) ejection and (**b**) sweep events.; Probability density function of the wall-normal lengths of (**c**) ejection and (**d**) sweep events.; Probability density function of the streamwise lengths of (**e**) ejection and (**f**) sweep events.

The spatial features of the 2D LSMs were examined relative to the proposed formulas. The structures can be classified into attached and detached structures relative to the minimum y-position of structure y_{min}, where $y_{min} \approx 0$ refers to wall-attached structures, whereas $y_{min} > 0$ refers to detached structures. That is, attached structures signify that the structure attaches to the wall, whereas detached structures suspend in the flow field. Herein, these identified structures were further classified into wall-attached and wall-detached structures, and the relationship between their characteristic lengths in streamwise and wall-normal directions is discussed.

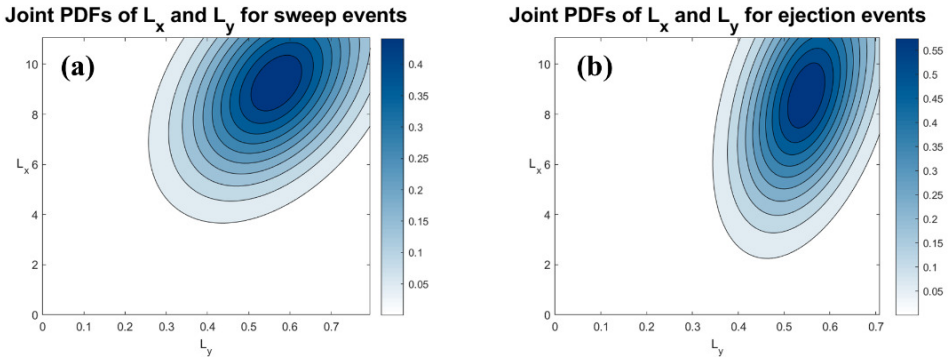

Figure 7. Joint PDFs of L_x and L_y of (**a**) sweep and (**b**) ejection events.

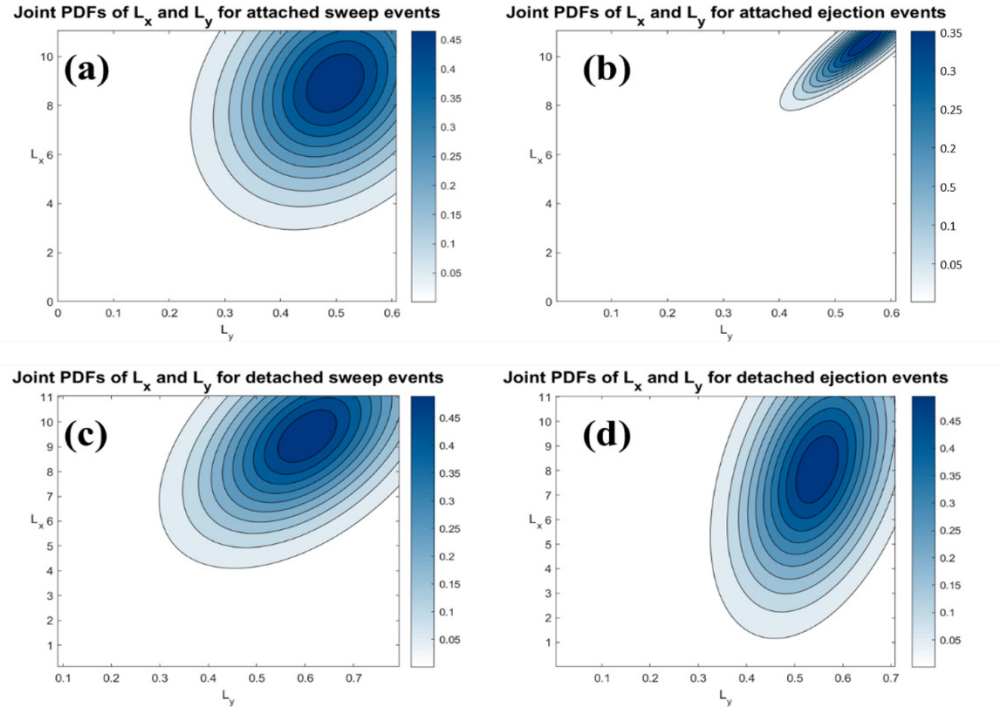

Figure 8. Joint PDFs of L_x and L_y of (a) attached sweep, (b) attached ejection, (c) detached sweep, and (d) detached ejection events.

Figure 7 presents the joint PDFs of L_x and L_y of sweep and ejection events. The slope of the joint PDF of ejection events is more tilted than that of sweep events, revealing that the vertical variation of sweep events is more extensive than that of ejection events. However, ejection events tend to exhibit more extended variation than do sweep events in the streamwise direction. That is, as a sweep event occurs, its streamwise length will generally exceed that of an ejection event, which is consistent with the findings of Dennis and Nickels (2011).

The results presented in **Figure 8**(a) and (c) indicate that despite the almost complete lack of distinction between the distributions of attached or detached sweep events, the distribution of detached sweep events is more similar to the distribution of entire sweep events. This phenomenon indirectly confirms the finding that sweep events appear away from the wall and drop to dissipate. Accordingly, sweep events are commonly named detached structures. By contrast, attached and

detached ejection events exhibit different distribution trends, as displayed in **Figure 8**(b) and (d). As presented in **Figure 8**(b), while the attached ejection event occurs, its spatial distribution tends to become more significant in both directions, which is consistent with the tall wall-attached structures observed by Yoon et al. (2020). The distributions of sweep and ejection events are similar to the distributions of detached sweep and ejection events, respectively.

7.2 Duration of LSMs and the Occurrence Ratio of Sweep Events to Ejection Events

Although ejection and sweep event durations can be determined using quadrant analysis or other criteria as each event passes through a single measurement point, the duration of the persistence of such events is difficult to be obtained using a point-wise measurement because an event may continue after a single measurement point passes.

Laskari et al. (2018) studied the time evolution of UMZs in the TBL and provided a residence time for LSMs. The concept of residence time differs considerably from the concepts of duration and lifespan. Liu et al. (2016) provided a sketch of duration, maximum shear stress, transport momentum, and period. Residence time is not identical to a period, which is the interval between two events. Herein, the duration of every event is directly tracked using the JHTDB, which yields the result presented in **Figure 9**.

Both events exhibit similar residence time distributions. Noguchi and Nezu (2009) also observed that both events exhibit similar duration distributions. In the current analysis, the duration distributions of ejection and sweep events are nearly identical. Consistent with the observation of Noguchi and Nezu (2009), the lifespan of coherent structures is a lognormal distribution.

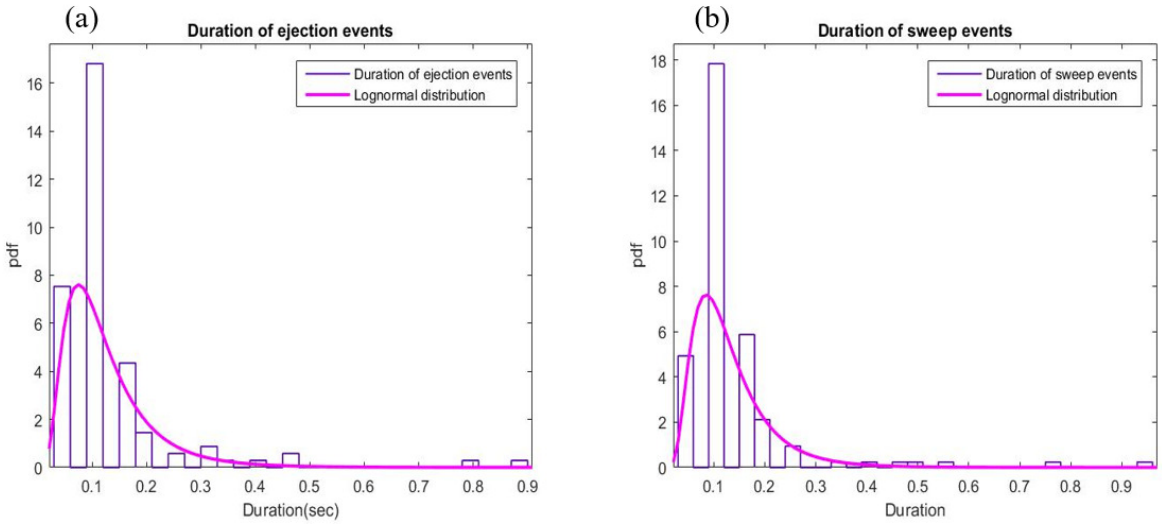

Figure 9. The probability density function of the duration (lifespan) of (**a**) ejection and (**b**) sweep events.

Regarding the occurrence ratio of ejection and sweep events along the normal-wall direction, Sun et al. (2019) observed that both the ratio of the ejection number to the total number of ejection and sweep events and that of the sweep number to the total number of ejection and sweep events declined with the increase of the wall-normal position in clear water condition. The number of ejection events was lower than that of sweep events; that is, the occurrence ratio of sweep events was higher than that of ejection events, which is consistent with the information we

extracted from the JHTDB (the occurrence ratio of sweep events was approximately 55-60%). In UMZs, an ejection event is not guaranteed to occur when a sweep event occurs. Moreover, we also determined an occurrence ratio of sweep events of 55%–60% under the condition that both ejection and sweep events have already occurred in each UMZ edge. **Table 2** summarizes the observations on the sweep and ejection events from the DNS data in this study.

Table 2. Characteristics of Q_2 and Q_4 events

Characterization of Q_2 and Q_4 events	**Observations**	
	Q_2 (Ejection event)	Q_4 (Sweep event)
Location of event occurrences	y^+ between 1100 and 2200 below the UMZ edges	y^+ above 4,400 above the UMZ edges
Attached and detached events	Primarily attached events (appear in the near-wall)	Primarily detached events (appear away from the wall)
Joint PDFs of L_x and L_y	more extensive in vertical variation	longer streamwise length
PDF of event durations	lognormal distribution	lognormal distribution
Occurrence Ratio	40%~45%	55%~60%

8. Conclusions

The existence of UMZs has been demonstrated to be crucial when determining the spatial distribution of coherent structures of LSMs in wall-bounded turbulence. Most studies have emphasized that LSMs such as ejection and sweep events in turbulence contribute to the probabilistic behaviors of turbulence, and subsequently, transport of sediment particles. Therefore, in the current study, conditional velocity decomposition in which the mean velocity is a function of wall-normal distance and UMZ edge height was used to capture coherent structures in the flow field. The structure of the wall-bounded turbulent flow based on the DNS data established by Lee and Moser (2014) was analyzed in this study.

In the current study, several criteria for identifying the turbulent coherent structures are revisited. A standard procedure that focuses on the spatial-temporal distribution of ejection and sweep events in wall-bounded flow is established. Fiscaletti and Ganapathisubramani (2018) proposed a criterion for distinguishing two arbitrary structures at two consecutive time steps, which we used to track the duration of each structure. This criterion was also used to discriminate and extract structures throughout the flow field in a single timestep. LSMs were then reliably extracted from wall-bounded turbulent flow and tracked by applying the integrated criteria as proposed in this study. Sweep and ejection event characterization, such as the probability distributions of event durations and streamwise length and wall-normal length, as well as the occurrence ratio, were quantified and then further compared with those reported in other studies.

Regarding the spatial properties of LSMs, the effect of the UMZ edges, which constrain the vertical development of LSMs, was considered. The scale of the wall-normal length (L_y) was consistent with that of observations of other wall-bounded flow. Yoon et al. (2020) revealed that most L_y ranges from 0.4δ to 0.6δ. However, some disparity was observed between our analysis and that of Dennis and Nickels (2011), which might be attributed to the essential difference in their flow conditions. The probability distributions of the maximum height, wall-normal length and

streamwise length of the coherent structures can be determined. Moreover, the joint probability distributions of the wall-normal and streamwise length of the sweep and ejection events respectively can be further established.

It is discovered that the distribution of detached sweep events is more similar to the distribution of entire sweep events. This phenomenon confirms the finding that sweep events appear away from the wall and drop to dissipate. Accordingly, sweep events are commonly named detached structures. By contrast, attached and detached ejection events exhibit different distribution trends. While the attached ejection event occurs, its spatial distribution tends to become larger in both directions. However, despite the spatial-resolution of LSMs being insufficient for capturing the real distribution of the streamwise length of structures because of its tendency to merge two structures in the streamwise direction, our observation confirms that VLSMs consist of LSMs. This result further reveals that LSM duration follows a lognormal distribution based on best fit, which is consistent with Noguchi and Nezu's (2009) findings. It is also found that an occurrence ratio of sweep events of 55%–60% under the condition that both ejection and sweep events can be observed occurred in each UMZ edge.

The organized vortical structures that contort UMZ interfaces are a manifestation of ejection events and sweep events around the interface, demonstrating that UMZ edges and the spatial distribution of LSMs affect each other. In this study, discrimination of the interfaces of UMZs is viewed as an essential step in estimating the spatial and temporal scales and other properties of LSMs. It is expected that our understanding of probabilistic characteristics of sweep and ejection coherent structures can be enhanced. With the better characterization of the random and intermittent behaviors of turbulent coherent structures, a complete description of sediment particle movement in turbulent flows can then be made available.

Acknowledgments

The authors thank the Ministry of Science and Technology of Taiwan for financially supporting this research under the contract numbers MOST 107-2628-E-002-002-MY3 and 108-2221-E-002-011-MY3. The authors would like to acknowledge the accessibility of the extensive database at Johns Hopkins Turbulence Database (JHTDB).

Data Availability

All the turbulence flow data used in this study are available at the Johns Hopkins Turbulence Database website funded by National Science Foundation http://turbulence.pha.jhu.edu.

549 **References**

550 Adrian, R., Christensen, K., & Liu, Z.-C. (2000). Analysis and interpretation of instantaneous
551 turbulent velocity fields. Experiments in Fluids, 29(3), 275-290.

552 Adrian, R. J., & Marusic, I. (2012). Coherent structures in flow over hydraulic engineering surfaces.
553 Journal of Hydraulic Research, 50(5), 451-464.

554 Adrian, R. J., Meinhart, C. D., & Tomkins, C. D. (2000). Vortex organization in the outer region
555 of the turbulent boundary layer. Journal of Fluid Mechanics, 422, 1-54.

556 Antonia, R. (1972). Conditionally sampled measurements near the outer edge of a turbulent
557 boundary layer. Journal of Fluid Mechanics, 56(1), 1-18.

558 Antonia, R., Prabhu, A., & Stephenson, S. (1975). Conditionally sampled measurements in a
559 heated turbulent jet. Journal of Fluid Mechanics, 72(3), 455-480.

560 Blackwelder, R. F., & Eckelmann, H. (1979). Streamwise vortices associated with the bursting
561 phenomenon. Journal of Fluid Mechanics, 94(3), 577-594.

562 Cellino, M., & Lemmin, U. (2004). Influence of coherent flow structures on the dynamics of
563 suspended sediment transport in open-channel flow. Journal of Hydraulic Engineering, 130(11),
564 1077-1088.

565 Chang, W., Constantinescu, G., Tsai, W., & Lien, H. (2011). Coherent structure dynamics and
566 sediment erosion mechanisms around an in-stream rectangular cylinder at low and moderate angles
567 of attack. Water Resources Research, 47(12).

568 Chen, D., Sun, H., & Zhang, Y. (2013). Fractional dispersion equation for sediment suspension.
569 Journal of Hydrology, 491, 13-22.

570 Chen, Q., Zhong, Q., Qi, M., & Wang, X. (2015). Comparison of vortex identification criteria for
571 planar velocity fields in wall turbulence. Physics of Fluids, 27(8), 085101.

572 de Silva, C. M., Hutchins, N., & Marusic, I. (2016). Uniform momentum zones in turbulent
573 boundary layers. Journal of Fluid Mechanics, 786, 309.

574 de Silva, C. M., Philip, J., Hutchins, N., & Marusic, I. (2017). Interfaces of uniform momentum
575 zones in turbulent boundary layers.

576 Dennis, D. J., & Nickels, T. B. (2011). Experimental measurement of large-scale three-dimensional
577 structures in a turbulent boundary layer. Part 2. Long structures. Journal of Fluid Mechanics, 673,
578 218.

579 Dwivedi, A., Melville, B. W., Shamseldin, A. Y., & Guha, T. K. (2011). Flow structures and
580 hydrodynamic force during sediment entrainment. Water Resources Research, 47(1).

581 Eisma, J., Westerweel, J., Ooms, G., & Elsinga, G. E. (2015). Interfaces and internal layers in a
582 turbulent boundary layer. Physics of Fluids, 27(5), 055103.

583 Fabris, G. (1979). Conditional sampling study of the turbulent wake of a cylinder. Part 1. Journal
584 of Fluid Mechanics, 94(4), 673-709.

585 Falco, R. E. (1977). Coherent motions in the outer region of turbulent boundary layers. The Physics
586 of Fluids, 20(10), S124-S132.

587 Ferreira, R., Leal, J., & Cardoso, A. (2002). Turbulent structures and near-bed sediment transport

588 in open-channel flows. River Flow 2002, 1, 553-563.

589 Fiscaletti, D., & Ganapathisubramani, B. (2018). Characteristics of sources and sinks of
590 momentum in a turbulent boundary layer. Physical Review Fluids, 3(5), 054601.

591 Franca, M. J., Santos, B., Antico, F., & Ferreira, R. (2014). Quadrant analysis of shear events in
592 open channel flows over mobile and immobile hydraulically rough beds. ERCOFTAC Bulletin,
593 100(ARTICLE), 29-36.

594 Ganapathisubramani, B., Longmire, E. K., & Marusic, I. (2003). Characteristics of vortex packets
595 in turbulent boundary layers.

596 Grass, A. J. (1971). Structural features of turbulent flow over smooth and rough boundaries.
597 Journal of Fluid Mechanics, 50(2), 233-255.

598 Gutmark, E., & Wygnanski, I. (1976). The planar turbulent jet. Journal of Fluid Mechanics, 73(3),
599 465-495.

600 Hedleyt, T. B., & Keffer, J. F. (1974). Some turbulent/non-turbulent properties of the outer
601 intermittent region of a boundary layer. Journal of Fluid Mechanics, 64(4), 645-678.

602 Hurther, D., & Lemmin, U. (2003). Turbulent particle flux and momentum flux statistics in
603 suspension flow. Water Resources Research, 39(5).

604 Hutchins, N., & Marusic, I. (2007). Large-scale influences in near-wall turbulence. Philosophical
605 Transactions of the Royal Society A: Mathematical, Physical and Engineering Sciences, 365(1852),
606 647-664.

607 JCR, H., Wray, A., & Moin, P. (1988). Eddies, stream, and convergence zones in turbulent flows.
608 Center for turbulence research report CTR-S88, 193-208.

609 Jeong, J., & Hussain, F. (1995). On the identification of a vortex. Journal of fluid mechanics, 285,
610 69-94.

611 Jeong, J., Hussain, F., Schoppa, W., & Kim, J. (1997). Coherent structures near the wall in a
612 turbulent channel flow. Journal of Fluid Mechanics, 332(185-214), 188.

613 Juan, C., ALAMO, J. J. E., Jiménez, J., Zandonade, P., & Moser, R. (2006). Self-similar vortex
614 clusters in the turbulent logarithmic region. J. Fluid Mech, 561, 329-358.

615 Kaftori, D., Hetsroni, G., & Banerjee, S. (1994). Funnel-shaped vortical structures in wall
616 turbulence. Physics of Fluids, 6(9), 3035-3050.

617 Kim, K., & Adrian, R. (1999). Very large-scale motion in the outer layer. Physics of Fluids, 11(2),
618 417-422.

619 Kwon, Y., Hutchins, N., & Monty, J. (2016). On the use of the Reynolds decomposition in the
620 intermittent region of turbulent boundary layers. Journal of Fluid Mechanics, 794, 5.

621 Laskari, A., de Kat, R., Hearst, R. J., & Ganapathisubramani, B. (2018). Time evolution of uniform
622 moment zones in a turbulent boundary layer.

623 Lee, J., Sung, H. J., & Zaki, T. A. (2017). Signature of large-scale motions on turbulent/non-
624 turbulent interface in boundary layers. Journal of Fluid Mechanics, 819, 165.

625 Lee, M., & Moser, R. D. (2014). Direct numerical simulation of turbulent channel flow up to
626 $\mathrm{Re}_\tau \approx 5200$. Journal of Fluid Mechanics. 774, 395-415.

LeHew, J., Guala, M., & McKeon, B. (2013). Time-resolved measurements of coherent structures in the turbulent boundary layer. Experiments in Fluids, 54(4), 1-16.

Lelouvetel, J., Bigillon, F., Doppler, D., Vinkovic, I., & Champagne, J. Y. (2009). Experimental investigation of ejections and sweeps involved in particle suspension. Water Resources Research, 45(2).

Liu, D., Liu, X., Fu, X., & Wang, G. (2016). Quantification of the bed load effects on turbulent open-channel flows. Journal of Geophysical Research: Earth Surface, 121(4), 767-789.

Lozano-Durán, A., Flores, O., & Jiménez, J. (2012). The three-dimensional structure of momentum transfer in turbulent channels, Journal of Fluid Mechanics, 694, 100.

Lozano-Durán, A., & Jiménez, J. (2014). Time-resolved evolution of coherent structures in turbulent channels: characterization of eddies and cascades. Journal of fluid mechanics, 759, 432.

Lu, S., & Willmarth, W. (1973). Measurements of the structure of the Reynolds stress in a turbulent boundary layer. Journal of Fluid Mechanics, 60(3), 481-511.

MacVicar, B., & Roy, A. (2007). Hydrodynamics of a forced riffle pool in a gravel bed river: 2. Scale and structure of coherent turbulent events. Water Resources Research, 43(12).

Meinhart, C. D., & Adrian, R. J. (1995). On the existence of uniform momentum zones in a turbulent boundary layer. Physics of Fluids, 7(4), 694-696.

Moisy, F., & Jiménez, J. (2004). Geometry and clustering of intense structures in isotropic turbulence. Journal of fluid mechanics, 513, 111.

Muste, M., Yu, K., Fujita, I., & Ettema, R. (2005). Two-phase versus mixed-flow perspective on suspended sediment transport in turbulent channel flows. Water Resources Research, 41(10).

Nagaosa, R. (1999). Direct numerical simulation of vortex structures and turbulent scalar transfer across a free surface in a fully developed turbulence. Physics of Fluids, 11(6), 1581-1595.

Nezu, I., Nakagawa, H., & Jirka, G. H. (1994). Turbulence in open-channel flows. Journal of Hydraulic Engineering, 120(10), 1235-1237.

Nino, Y., & García, M. (1996). Heuristic model for particle entrainment into suspension. Proceedings of the 1996 11th Conference on Engineering Mechanics. Part 1 (of 2),

Noguchi, K., & Nezu, I. (2009). Particle–turbulence interaction and local particle concentration in sediment-laden open-channel flows. Journal of Hydro-environment Research, 3(2), 54-68.

Offen, G., & Kline, S. (1975). A proposed model of the bursting process in turbulent boundary layers. Journal of Fluid Mechanics, 70(2), 209-228.

Okamoto, T., Nezu, I., & Katayama, A. (2010). Simultaneous measurements of concentration and velocity with combined PIV and planar LIF in vegetated open-channel flows. River Flow 2010, 487-494.

Robinson, S. K. (1991). Coherent motions in the turbulent boundary layer. Annual Review of Fluid Mechanics, 23(1), 601-639.

Salim, S., Pattiaratchi, C., Tinoco, R., Coco, G., Hetzel, Y., Wijeratne, S., & Jayaratne, R. (2017). The influence of turbulent bursting on sediment resuspension under unidirectional currents. Earth Surface Dynamics, 5(3), 399-415.

Saxton-Fox, T., & McKeon, B. J. (2017). Coherent structures, uniform momentum zones and the streamwise energy spectrum in wall-bounded turbulent flows. Journal of Fluid Mechanics, 826.

Séchet, P., & le Guennec, B. (1999). The role of near wall turbulent structures on sediment transport. Water Research, 33(17), 3646-3656.

She, Z.-S., Jackson, E., & Orszag, S. A. (1990). Intermittent vortex structures in homogeneous isotropic turbulence. Nature, 344(6263), 226-228.

Smits, A. J., McKeon, B. J., & Marusic, I. (2011). High–Reynolds number wall turbulence. Annual Review of Fluid Mechanics, 43, 353-375.

Srinath, S. (2017). Modeling and prediction of near wall turbulent flows Ecole Centrale de Lille].

Sun, J., Gao, T., Fan, Y., Chen, W., & Xuan, R. (2019). The modulation of particles on coherent structure of turbulent boundary layer in dilute liquid-solid two-phase flow with PIV. Powder Technology, 344, 883-896.

Tomkins, C. D., & Adrian, R. J. (2002). Spanwise structure and scale growth in turbulent boundary layers (0073-5264).

Truong, S., & Uijttewaal, W. (2019). Transverse momentum exchange induced by large coherent structures in a vegetated compound channel. Water Resources Research, 55(1), 589-612.

Tsai, C. W., & Huang, S. H. (2019). Modeling suspended sediment transport under influence of turbulence ejection and sweep events. Water Resources Research, 55(7), 5379-5393.

Tsai, C. W., Huang, S. H., & Hung, S. Y. (2021). Incorporating the Memory Effect of Turbulence Structures into Suspended Sediment Transport Modeling. Water Resources Research, 57(3), e2020WR028475.

Wallace, J. M., Eckelmann, H., & Brodkey, R. S. (1972). The wall region in turbulent shear flow. Journal of Fluid Mechanics, 54(1), 39-48.

Wang, F., Huai, W., Guo, Y., & Liu, M. (2021). Turbulence Structure and Momentum Exchange in Compound Channel Flows with Shore Ice Covered on the Floodplains. Water Resources Research, 57(4), e2020WR028621.

Yoon, M., Hwang, J., Yang, J., & Sung, H. J. (2020). Wall-attached structures of streamwise velocity fluctuations in an adverse-pressure-gradient turbulent boundary layer. Journal of Fluid Mechanics, 885.

Zhong, Q., Chen, Q., Wang, H., Li, D., & Wang, X. (2016). Statistical analysis of turbulent super-streamwise vortices based on observations of streaky structures near the free surface in the smooth open channel flow. Water Resources Research, 52(5), 3563-3578.

Zhou, J., Adrian, R. J., Balachandar, S., & Kendall, T. (1999). Mechanisms for generating coherent packets of hairpin vortices in channel flow. Journal of Fluid mechanics, 387, 353-396.